Analysis of the short-range order of the Au/Fe(001) surface alloy

M. M. J. Bischoff, T. K. Yamada, and H. van Kempen*
NSRIM, University of Nijmegen, Toernooiveld 1, NL-6525 ED Nijmegen, The Netherlands
(Received 17 September 2002; revised manuscript received 15 January 2003; published 2 April 2003)

Scanning tunneling microscopy measurements show that the growth of about half a monolayer Au on Fe(001) at a temperature of 170 °C leads after a postanneal at 700 °C to an island free and homogeneously alloyed surface layer. The surface alloying is in contrast to the bulk where Au and Fe are immiscible. Strong chemical contrast in the images allows us to analyze the short-range order of this surface alloy. Two independent methods are considered: the first method extracts pair occupation probabilities directly from digitized images, the second method makes use of the autocorrelation of filtered images. Both methods lead to the same conclusion: only for the nearest-neighbor sites a strong preference for unlike species is found; for further sites the probabilities follow a random distribution. Scanning tunneling spectroscopy measurements on the alloyed AuFe surface are used to corroborate the interpretation of the chemical contrast. Furthermore, the spectroscopy results show that the Fe(001) surface state shifts to higher energies on areas where pure Fe patches are confined by Au atoms.

DOI: 10.1103/PhysRevB.67.165403 PACS number(s): 68.35.Bs, 68.37.Ef, 73.20.At

I. INTRODUCTION

In a recent publication we showed that the roughening of the Au(001)/Fe(001) interface is a result of the creation and annihilation of a surface-confined alloy during growth of this system.[1] Scanning tunneling microscopy (STM) images with chemical contrast revealed that for growth temperatures above 100 °C and coverages below 0.5 ML Au atoms become incorporated in the Fe(001) surface despite the immiscibility of Au in bulk Fe.[2] Growth of about 0.5 ML Au around 200 °C was found to lead to a homogeneously alloyed surface layer. However, if more Au is added, the surface-confined nature of the alloy[3] leads to a demixing with a roughened interface as a natural consequence. Understanding of the processes driving the surface alloying/dealloying and consequently the interface roughening are important since the quality of the interface, i.e., sharp/rough, mixed/pure, determines to a large degree the transport and magnetic properties of multilayer devices. In this perspective, the Au/Fe system can be considered as a perfect model system. However, to come to a better understanding of these phenomena a thorough characterization of the Au-Fe surface alloy is necessary.

In the present paper we make use of STM images which show chemical contrast to analyze the short-range order of the Au/Fe surface alloy. For this purpose, two methods of analysis are considered. The first method obtains the pair occupation probabilities directly from the STM images. This kind of analysis was, e.g., presented by Davies *et al.* for the Cr/Fe(001) surface alloy.[4] The second method makes use of the autocorrelation of the STM images and was described in detail by Hebenstreit *et al.*[5] and Schmid[6].

The surface state of the Fe(001) surface which appears as a strong peak in the spectroscopic dI/dV curve[7–10] can be used as a chemical fingerprint of local Fe areas as was successfully shown by Davies *et al.* in the case of Cr on Fe(001).[11] Also, in the present study scanning tunneling spectroscopy (STS) is used to corroborate the interpretation of the chemical contrast. Furthermore, it will be examined how the Fe(001) surface state is influenced by the alloying.

II. EXPERIMENTAL DETAILS

The experiments were performed in a home-built ultrahigh vacuum (UHV) system consisting of a fast-entry loadlock, a preparation chamber and an analysis chamber. The preparation chamber has a base pressure of about 1×10^{-10} mbar and contains equipment for sample cleaning, electron beam heating, epitaxial growth, and Auger electron spectroscopy (AES). The analysis chamber which contains the STM has a base pressure of less than 5×10^{-11} mbar.

A single-crystal Fe(001) whisker with a size of about $7\times1\times1$ mm^3 was used as the sample. In the early stage of the cleaning process, AES showed that oxygen and carbon impurities preferentially segregate to the surface at temperatures between 200 °C and 300 °C. The AES signals of these impurities were found to decrease again at higher annealing temperatures. Therefore, in order to get rid of these bulk impurities most efficiently the ion bombardment (750 eV Ar^+) was performed while ramping the annealing temperature between 150 °C and 750 °C. The sample temperature of 750 °C was verified with an infrared pyrometer. After a few days of these cycles, only oxygen could be detected by AES. The ratio of the oxygen and iron peaks was about 2% at this stage. From the concentration of depressions in the STM images, this ratio can be translated into an oxygen coverage of about 1%. After this bulk-depletion stage, the whisker was sputtered for about 45 min at 750 °C before the actual measurement. The radiative cooling time to room temperature was sufficient to repair any sputter damage as verified by the STM measurements which generally show terraces wider than 200 nm. This treatment also kept the surface impurity concentration below 1%.

Gold (99.99% pure) was evaporated from a Knudsen cell which is shielded by a liquid nitrogen cooled shroud. This keeps the pressure in the low 1×10^{-10} mbar range during

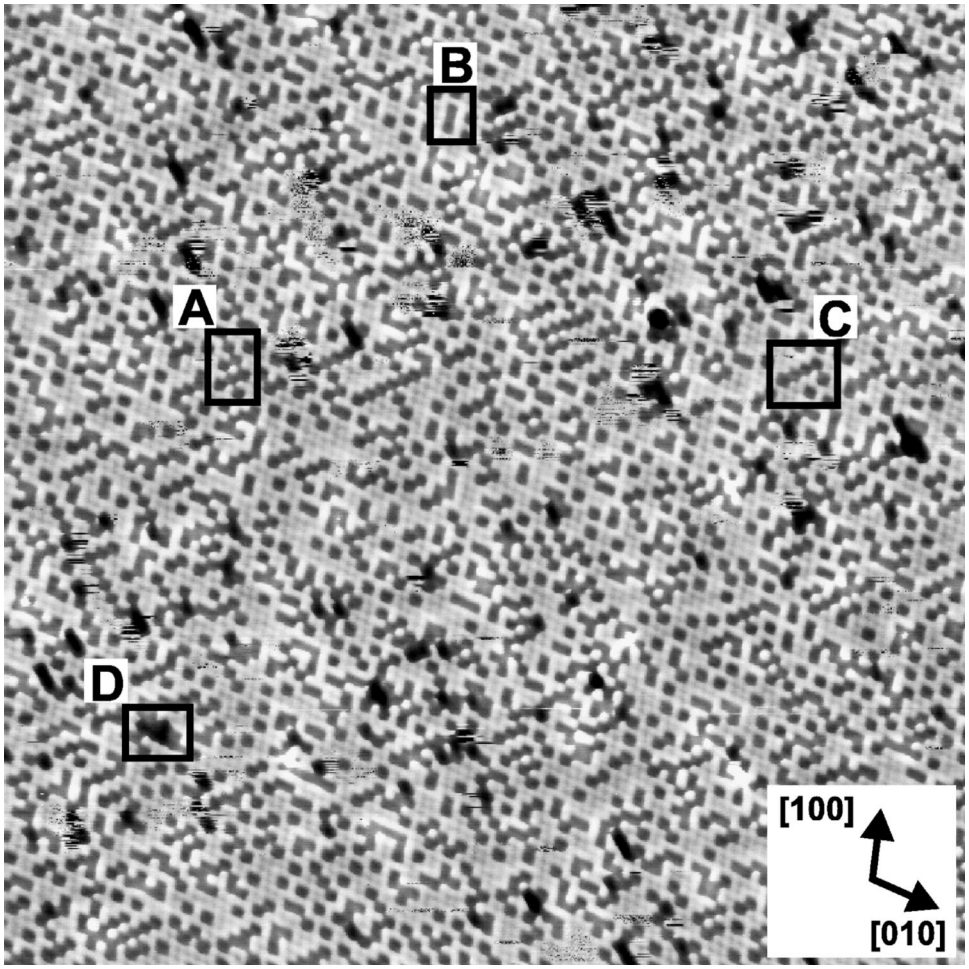

FIG. 1. Chemically resolved STM image of the Fe(001) surface which was covered with 0.5 ML Au and postannealed at 700 °C (30 nm $\times$30 nm, -0.28 V, 0.10 nA). 60 pm depressed lattice sites can be observed in this image which show an apparent short-range order: The areas marked *"A"*, *"B"*, and *"C"* show a local $c(2\times2)$ ordered area, a line along the close-packed [100] direction, and a line along the [110] direction, respectively. *"D"* shows one of the deeper and larger depressions, which are attributed to impurities.

growth. The evaporation rate was typically 0.2 monolayer/min as determined by a quartz crystal microbalance and histograms of STM images obtained after submonolayer growth of Au at temperatures below 100 °C. Here one monolayer (ML) is defined as a complete overlayer with Fe(001) bulk lattice constant (1.214×10^{19}atoms m^{-2}). During growth, the substrate can be resistively heated to a maximum temperature of about 250 °C. The sample temperature during growth was measured by a thermocouple mounted close to (but not in direct contact with) the sample making the inaccuracy in these temperature measurements large (±30 °C).

The STM experiments were performed with an Omicron UHV STM-1 operating at room temperature. Electrochemically etched *W* tips were cleaned and sharpened *in situ* by Ar self-sputtering. During the STM measurements, the tips were often ''reconditioned'' by applying voltage pulses of ±10 V at about 0.1 nA. To be able to compare topographic features with spectroscopic ones, STS measurements were performed simultaneously with conventional constant current images: at each pixel the feedback loop was temporarily switched off to record an $I(V)$ curve. These images were measured at a reduced resolution of typically 75×75 pixels to avoid strong distortions due to drift. The images presented in this paper were not corrected for drift. The $I(V)$ curves were numerically differentiated using a five-point window to obtain dI/dV.

III. RESULTS AND DISCUSSION

In Ref. 1 we showed that for submonolayer growth of Au (coverages below 0.5 ML) bright features appeared in the Fe(001) terrace for growth temperatures above 100 °C. Since the concentration of these features increased with growth temperature and Au coverage, we identified them as Au atoms which have place exchanged with substrate Fe atoms. For growth of about 0.5 ML Au at about 200 °C a homogeneously alloyed overlayer was found. Nevertheless, this alloyed overlayer apparently did not show any long-range order. To study this overlayer in detail, 0.5 ML of Au is grown on Fe(001) at a substrate temperature of 170 °C. In contrast to the experiments in Ref. 1, after growth we postannealed the sample for 1 h at a temperature of 700 °C. The motivation for this postannealing step was to see whether this treatment could result in an ordered surface alloy. Furthermore, postannealing reduces the island density which facilitates the analysis. The sample was radiatively cooled down to room temperature after the annealing step. Figure 1 shows an atomically and chemically resolved STM image of the surface after this preparation. It must be noted that this strong chemical contrast is only achieved with special tip conditions. Possibly, in this case an adsorbate at the tip apex interacts differently with the various species of surface atoms.[12] This contrast does not show any strong influence of

TABLE I. Pair occupation probabilities for equivalent surface near-nearest neighbor sites (up to fifth nearest neighbor). Three STM images are analyzed and are labeled "1", "2", and "3" for convenience. However, only the image labeled "1" is shown in this paper (i.e., Fig. 1). C_{Au} and C_{Fe} are the Au and Fe concentrations, respectively. $P_{\mathrm{AuAu(n)}}$ and $P_{\mathrm{FeFe(n)}}$ are the probabilities to find a Au-Au or Fe-Fe pair at nth surface nearest-neighbor sites.

Image	C_{Au}	$P_{\mathrm{AuAu(1)}}$	$P_{\mathrm{AuAu(2)}}$	$P_{\mathrm{AuAu(3)}}$	$P_{\mathrm{AuAu(4)}}$	$P_{\mathrm{AuAu(5)}}$
1	0.265	0.162	0.323	0.268	0.256	0.262
2	0.270	0.151	0.286	0.270	0.271	0.271
3	0.279	0.160	0.292	0.278	0.280	0.289
	C_{Fe}	$P_{\mathrm{FeFe(1)}}$	$P_{\mathrm{FeFe(2)}}$	$P_{\mathrm{FeFe(3)}}$	$P_{\mathrm{FeFe(4)}}$	$P_{\mathrm{FeFe(5)}}$
1	0.735	0.695	0.756	0.732	0.730	0.730
2	0.730	0.688	0.739	0.730	0.730	0.731
3	0.721	0.680	0.733	0.721	0.724	0.728

the particular set points of tunneling current or bias voltage. No islands are visible after the high-temperature postannealing in contrast to the growth at about 200 °C.[1] The terraces show 60 pm deep depressions at the lattice sites of a weakly corrugated (<10 pm)$p(1\times1)$ lattice. A long-range ordering of the depressions is missing although locally small $c(2\times2)$ ordered patches (cf. the area marked "*A*"), lines along the close-packed [100] directions (cf. marked "*B*") and lines along second nearest-neighbor [110] directions (cf. marked "*C*") are often observed. The larger and deeper (about 100 pm deep) depressions (cf. marked "*D*") are attributed to oxygen impurities. Their concentration is about 1%. Furthermore, tip conditions not allowing chemical contrast image them as well.

STM images like Fig. 1 are digitized by manually transforming the square lattice into an $m\times n$ (with m,n typically around 50) matrix of which each element (corresponding to a lattice site) can possess only three height values: "0" if the site is occupied by an impurity, "1" if occupied by a bright atom, and "2" if occupied by a depressed atom. From these matrices the surface coverage of the two species (C_{Au} and C_{Fe}) and the pair occupation probabilities for equivalent ($P_{\mathrm{AuAu(n)}}$ and $P_{\mathrm{FeFe(n)}}$) and inequivalent surface near-neighbor sites ($P_{\mathrm{AuFe(n)}}$ and $P_{\mathrm{FeAu(n)}}$) can be determined. Near-neighbor sites up to the fifth nearest neighbor ($n=5$) are considered. Sites having impurities at near-neighbor sites closer than five times the nearest-neighbor distance are discarded from the analysis. The results of this analysis are shown in Table I for three STM images. First, it follows that the concentration of the depressed sites in Fig. 1 is 0.265 ML. From this it can be concluded that the depressed lattice sites are the Au atoms, since only 0.50 ML Au was deposited. It also means that about half of the deposited Au disappears into the bulk after the high-temperature postannealing step. Table I shows that only the pair occupation probabilities for equivalent nearest- and next-nearest-neighbor sites deviate from a random distribution for which

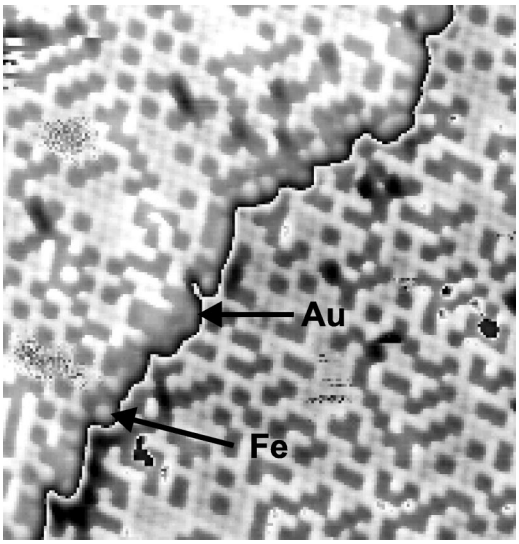

FIG. 2. Topographic STM image showing chemical contrast across a step edge (11 nm×11 nm, −0.28 V, 0.10 nA). The Au and Fe atoms at the step edge are marked. A stepped linear gray scale has been used: the black-white range corresponds to about 0.15 nm on both terraces. The black (white) perimeter along the step edge is a gray scale artifact.

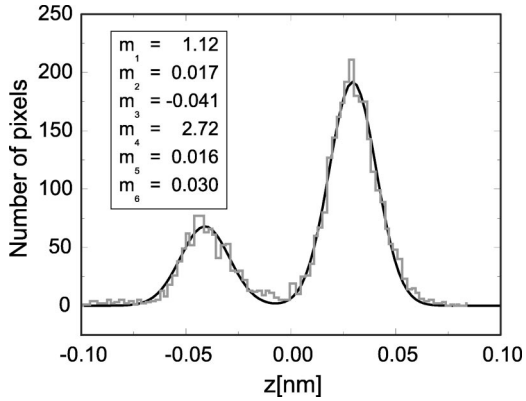

FIG. 3. Histogram of the apparent heights of the pixels corresponding to the atom positions of Fig. 1 (gray curve). This histogram is fitted to a sum of two Gaussians (black curve). The results for the fitting parameters m_1–m_6 are shown as well. The Au coverage can be determined from the ratio between the Gaussian peak amplitudes: $C_{\mathrm{Au}}=1-m_4/(1+m_4)$.

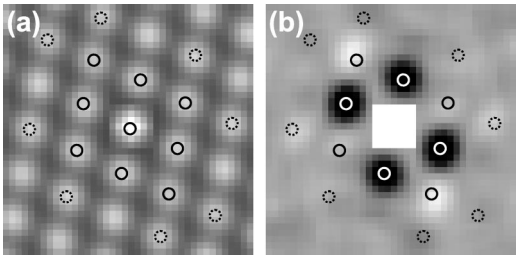

FIG. 4. Autocorrelation analysis of STM image with chemical contrast (Fig. 1). The STM image is modified as described in the text. (a) shows the autocorrelation of the atomic image (i.e., all atoms have the same height). (b) shows the autocorrelation of the chemical image (the Au and the Fe atoms have a different height). The white square in the center of the image is a gray scale artifact [$AC(0)$ is one, while at the other lattice sites it is much lower]. Equivalent points in these images are marked. White circles correspond to $AC(1)$, black circles to $AC(2)$, dotted circles to $AC(4)$. See text for discussion.

$P_{\mathrm{AuAu(n)}}$ ($P_{\mathrm{FeFe(n)}}$) would be simply C_{Au} (C_{Fe}). More specifically, $P_{\mathrm{AuAu(1)}}$ is only $58\pm2\%$ of the value expected for a random distribution, while $P_{\mathrm{FeFe(1)}}$ is reduced to $94\pm1\%$. From these values it can be concluded that nearest neighbors of different species are preferred. The values for the second nearest neighbors are less different from a random distribution although there is a slight preference for equivalent species: $P_{\mathrm{AuAu(2)}}$ and $P_{\mathrm{FeFe(2)}}$ are $111\pm8\%$ and $102\pm1\%$ of the values expected for a random distribution. The probabilities for $n>2$ are equivalent to the random distribution within the accuracy of the analysis.

Figure 2 shows an atomically and chemically resolved STM image across a monoatomic step. It can be seen that the steps have a preference for Au atoms. About 80% of the step edge sites are occupied by Au atoms which is three times higher than the value expected for a random distribution.

To check the reliability of the results obtained above, the method based on the autocorrelation as described by Hebenstreit[5] and Schmid[6] is also used to analyze the short-range order of the Au-Fe surface alloy. For this purpose the chemically resolved STM image of Fig. 1 is first bandpass filtered to enhance the atomic lattice. A local maxima search is implemented to find the pixel positions of the atoms. The histogram of the apparent heights of these pixels is shown in Fig. 3 and shows two well-separated peaks. This histogram is fitted to a sum of two Gaussians,

$$f(x)=(m_1/m_2)\exp\{-[(z-m_3)/m_2]^2\} + (m_1m_4/m_5)\exp\{-[(z-m_6)/m_5]^2\}. \quad (1)$$

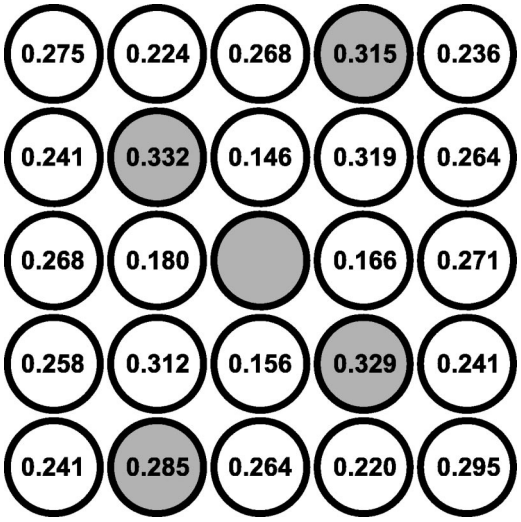

FIG. 5. Pair occupation probabilities for Au-Au pairs (image 1 of Table I) specified for each lattice direction. The values at the gray sites are slightly enhanced in agreement with the autocorrelation results of Fig. 4(b). The gray sites make up an apparent surface alloy unit cell with an Au concentration of 1/3.

The values of m_1–m_6 which are the results of the fitting procedure are shown in Fig. 3 as well. The Au concentration on the surface can be extracted from m_4,[5,6]

$$C_{\mathrm{Au}}=1-m_4/(1+m_4). \quad (2)$$

Thus, for the image of Fig. 1 we find an Au concentration of 0.269 which is in good agreement with the result obtained by the first (direct) method (see image ''1'' in Table I). The apparent height which separates the two histogram peaks (roughly -0.01 nm) is used as a discriminator: pixels with height smaller than this value are put at $-\sqrt{C_{\mathrm{Au}}/C_{\mathrm{Fe}}}$, while pixels with a larger height are put at $+\sqrt{C_{\mathrm{Fe}}/C_{\mathrm{Au}}}$.[5,6] Then, the single-pixel atom positions are broadened to 3×3 pixel clusters. The values of the remaining background pixels are put at a value that assures that the average of the total image is zero. The autocorrelation of this ''chemical'' image is calculated.

By setting the pixel clusters that describe the atom positions at equal values, the chemical information is lost. By definition, the autocorrelation of this ''atomic'' image must be one at lattice distances. However, deviations from a perfect square lattice (due to distortions) result in autocorrelations less than one. These deviations influence the autocorrelation of the chemical image equivalently. Therefore, to compensate for these errors the autocorrelation values obtained from the chemical image are normalized by the auto-

TABLE II. Autocorrelations (AC) for the five nearest-neighbor distances obtained directly from the chemically resolved STM image (Fig. 1) and obtained from the probabilities of Table I (averages of three images) and Eqs. (3) and (4).

	$AC(1)$	$AC(2)$	$AC(3)$	$AC(4)$	$AC(5)$
Direct calculation	-0.21 ± 0.01	$+0.04\pm0.02$	0	0	0
From probabilities	-0.16 ± 0.01	$+0.05\pm0.02$	0	0	0

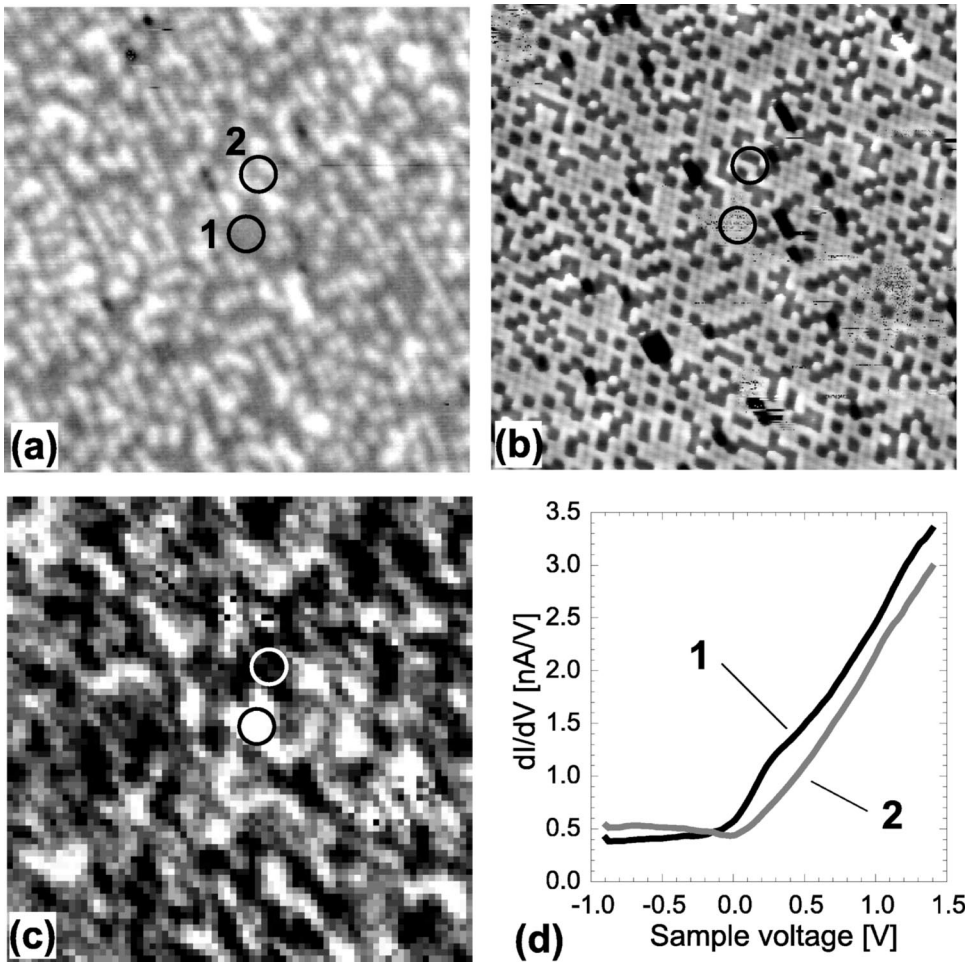

FIG. 6. (a) and (b) are consecutively obtained STM images of the same area of the Au-Fe surface alloy (15 nm×15 nm). The set points for these images are −1.0 V, 0.04 nA (a) and −0.28 V, 0.01 nA (b), respectively. A change of the tip apex configuration leads to a different contrast: the protrusions in (a) correspond to the dark lattice sites in (b). A spectroscopy measurement is performed at the same area ($V_s=-0.5$ V, $I=0.20$ nA). (c) shows the dI/dV map at $V_s=+0.20$ V. (d) shows dI/dV curves obtained by averaging the single dI/dV curves obtained in the encircled areas in Figs. 3(a)–3(c).

correlation values from the atomic image. Both autocorrelation images are shown in Fig. 4.

The interpretation of this method is as follows. An autocorrelation value of zero corresponds to a random distribution. An autocorrelation of $+1$ means that atoms of the same species are preferred, while a negative value means that atoms of different species are preferred. For the latter case, the minimum value is given by $1-1/C_{\mathrm{Fe}}$, i.e., -0.37 (-1 is only obtained for a perfectly ordered $c(2\times2)$ structure). Figure 4(b) shows that a large negative value for the autocorrelation (AC) is found at the nearest-neighbor distances. Averaging over the four equivalent sites gives $AC(1)=-0.21\pm0.01$. The autocorrelation of the averaged second nearest-neighbor sites is slightly positive: $AC(2)=+0.04\pm0.02$. The autocorrelations for larger distances average to zero. However, a more careful look at Fig. 4(b) reveals that there is a weak asymmetry in $AC(2)$ and $AC(4)$: slightly larger values are found at two diagonally linked sites for both $AC(2)$ and $AC(4)$.

Now the results of both methods can be compared by using the relation between the autocorrelations and the pair occupation probabilities,[5,6]

$$W_{\mathrm{diff}}(n)=2C_{\mathrm{Fe}}C_{\mathrm{Au}}[1-AC(n)]. \tag{3}$$

$W_{\mathrm{diff}}(n)$ is the probability to find a pair of different atoms at nth nearest-neighbor sites and can be expressed in the probabilities given in Table I,

$$W_{\mathrm{diff}}(n)=C_{\mathrm{Au}}P_{\mathrm{AuFe(n)}}+C_{\mathrm{Fe}}P_{\mathrm{FeAu(n)}}. \tag{4}$$

$P_{\mathrm{AuFe(n)}}$ and $P_{\mathrm{FeAu(n)}}$ are simply given by $1-P_{\mathrm{AuAu(n)}}$ and $1-P_{\mathrm{FeFe(n)}}$, respectively. Using the values of Table I, autocorrelation values are calculated from Eqs. (3) and (4). The results are shown in Table II together with the autocorrelations obtained from Fig. 4. It is clear that both methods lead to similar results.

To confirm whether the weak asymmetry in the $AC(2)$ and $AC(4)$ values is a real effect or an artifact of the analysis, the pair occupation probabilities for image 1 of Table I are specified for the different directions. Figure 5 shows that the asymmetries are also found in the directly obtained pair occupation probabilities. This seems to point at a unit cell for the surface alloy which contains 6 atoms of which 2 are Au. Remarkably, the Au concentration in this cell is 1/3 which is comparable to the Au concentration in the surface. Therefore, this cell might be the result of a balance between the Au surface concentration and repulsive Au-Au interactions. The asymmetry might be imposed by the monoatomic steps on the Fe(001) surface. Indeed, comparison with Fig. 2 shows that the short direction of the unit cell of the surface alloy is parallel to the step direction. The preference for Au atoms at the step edge sites might thus induce the observed asymmetry.

In contrast to the images shown in Ref. 1, in which only the Au atoms are visible, Figs. 1 and 2 show both species of

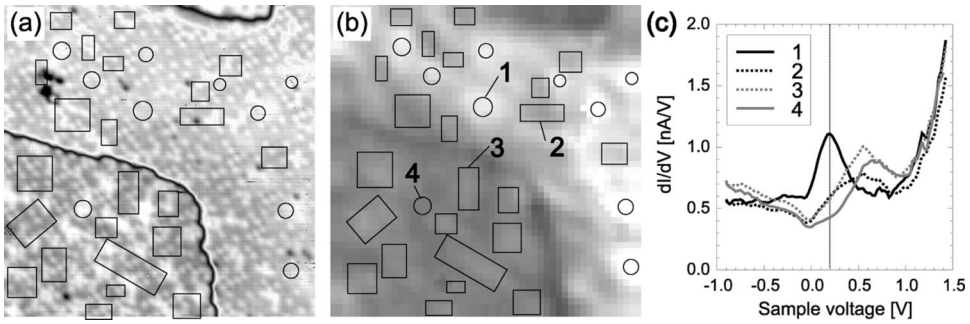

FIG. 7. STS measurement performed at Fe(001) covered with 0.35 ML Au at 200 °C. The size of (a) and (b) are 13 nm $\times$13 nm. (a) is the topographic image obtained at a set point of -0.01 V, 0.25 nA and (b) is the dI/dV map at $V_s=+0.20$ V. The spectroscopic measurement (set point: -1.0 V, 0.5 nA) was performed after the topographic image. Squares in (a) and (b) indicate equivalent areas. (c) shows four dI/dV curves that are representative of the four different contrasts in the dI/dV map. These curves are averages of the curves obtained within the labeled squares and circles (1–4).

the Au-Fe alloyed overlayer. Occasionally, changes in the tip configuration, probably caused by the exchange of the tip apex atom, lead to large changes in contrast. As an example, Figs. 6(a) and 6(b) show two consecutively obtained STM images of the same area. It is obvious that the 15 pm high protrusions in Fig. 6(a) correspond to the dark lattice sites in Fig. 6(b). Some adsorbates at the tip [e.g., in Fig. 6(a)] lead to a strong interaction with the embedded Au atoms causing an increase in the tunnel current, but not with the Fe atoms that are not resolved; other adsorbates [e.g., in Fig. 6(b)] cause an interaction that decreases the current at the Au atoms, which probably allows the tip to come close enough to the surface to resolve the Fe lattice.

Between the measurements of Figs. 6(a) and 6(b) an STS measurement was performed at the same area (set points: $V_s=-0.5$ V and $I=0.20$ nA). Figure 6(c) shows the dI/dV map at the bias voltage of $+0.20$ V. This voltage is chosen since Fe(001) is known to have a localized d_{z^2}-like surface state around this energy.[7–10] The dark areas in Fig. 6(a) are bright in the dI/dV map which gives additional evidence that the dark areas in Fig. 6(a) are the Fe atoms and the bright protrusions are the Au atoms. Also, since the dark atoms in Fig. 6(b) are positioned at the positions of the bright protrusions in Fig. 6(a), these dark atoms must be the Au atoms.

Two averaged dI/dV curves are shown in Fig. 6(d). The areas in which the pixels have been averaged to obtain these curves are marked in Figs. 6(a) to 6(c). Unfortunately, the tip leading to the strong atomical and chemical contrast does not allow the Fe(001) surface state to be resolved in the dI/dV curve as a peak due to the rapidly rising background with increasing voltage. Instead, only a shoulder is observed. The influence of the tip configuration on the background was previously discussed for STS experiments on Mn/Fe(001).[10]

The reversed contrasts of Figs. 6(a) and 6(b) show that a relation between the chemical contrast and the Fe(001) surface state is not straightforward. Both images are recorded at negative bias voltages, where the influence of the surface state on the electronic structure is negligible. Furthermore, these types of contrasts change frequently (when the tip condition is changed) and show no particular influence on the tunneling setpoints. In other words, no evidence was found that the chemical contrast is enhanced around the surface-state energy. Therefore, instead of explaining the chemical contrast in terms of the Fe(001) surface state, the best we can do at present is to identify both types of atoms by making use of the Fe(001) surface state.

Figure 7 shows STS results obtained with a tip showing the Au atoms as bright protrusions (set points: -0.01 V, 0.25 nA). For these measurements the postannealing step was not performed: 0.35 ML Au was grown on Fe(001) at a substrate temperature of 200 °C. For this preparation, the island coverage corresponds to the amount of Au. In this case, the dI/dV curves that are obtained on the same area as in Fig. 7(a) (but after the topographic image was obtained and with different set points: -1.0 V, 0.5 nA) show a largely suppressed background at the high-voltage side [e.g., Fig. 7(c)]. The dI/dV map at $V_s=+0.20$ V [Fig. 7(b)] shows bright and dark areas on both the terrace and the island. The island appears darker in the dI/dV map than the terrace that can be explained by the higher Au concentration in the island compared to the terrace for this particular preparation. However, it is not trivial to correlate the contrasts in the dI/dV map to the atomic scale features in Fig. 7(a). The reason is that the larger tunneling resistance during the spectroscopy measurements leads to a larger tip-sample distance which deteriorates the resolution (typically 0.7 nm, see e.g.[13–15]). Nevertheless, some tendencies can be recognized. To facilitate this purpose, equal areas are marked with squares and circles in Figs. 7(a) and 7(b). The brightest dI/dV map contrasts on the terrace are found at pure Fe(001) patches of at least 1 nm$\times$1 nm. Although less clear, the darkest dI/dV map contrasts on the terrace seem to be localized on areas which contain many Au atoms. The same conclusion can be drawn for the island: The brightest dI/dV map contrasts are found in areas which contain many dark spots (i.e. Fe), while the darkest dI/dV map contrasts on the island are found on close-packed areas of bright protrusions (Au).

Four dI/dV curves which are representative of these four different dI/dV map contrasts are shown in Fig. 7(c). Clearly, the pure Fe(001) patches reveal a strong peak at $+0.20$ V (e.g., curve ''1''). The areas of close-packed Au atoms on the island (e.g., ''4'') show the other extreme: a peak around $+0.70$ V. Curves ''2'' and ''3'' show peaks at energies between $+0.20$ and $+0.70$ V. It should be stressed that the dI/dV curves shown in Fig. 7(c) are only presenting four typical curves measured at this complex surface; curves ''1'' and ''4'' only represent the extremes that are observed.

Instead of relating the $+0.70$ V peak to the Au, it seems more reasonable to relate it to an upward shift of the d_{z^2} surface state of Fe(001). The incorporated Au atoms may confine the Fe(001) surface-state electrons to small patches thereby increasing their energy. The same kind of behavior was observed on a $Fe_{96.5}Si_{3.5}$ surface alloy:[8] here one-dimensional localization of the Fe(001) surface state on antiphase domain boundaries leads to an upward shift to $+0.6$ V. Geometrically, the local structure of these domain boundaries resemble the present local structures.

IV. CONCLUSION

We presented two independent analyses of the short-range order of the surface-confined AuFe alloy. This surface alloy was prepared by growth of about 0.5 ML Au on an Fe(001) whisker at a temperature of about 170 °C. After growth, the surface was annealed at 700 °C. A strong preference for unlike nearest-neighbor sites was found. The pair occupation probabilities for sites at larger distances follow a random distribution. Step sites have a strong preference for Au atoms. The interpretation of the Au and Fe atoms in the STM images with chemical contrast was corroborated by STS results which reveal the well-known Fe(001) surface state at areas as small as 1 nm^2. Upward peak shifts of the Fe surface state were found on small Fe areas which are enclosed by incorporated Au atoms. It is clear that this shift strongly depends on the local geometry, although, the typical resolution during STS measurements is too low to allow for a more precise determination.

ACKNOWLEDGMENTS

We would like to thank D. T. Pierce for kindly providing us with the Fe whiskers. This work was supported by the European Growth project MAGNETUDE and the Stichting voor Fundamenteel Onderzoek der Materie (FOM), which is funded by the Nederlandse Organisatie voor Wetenschappelijk Onderzoek (NWO).

*FAX: +31 24 3652190. Email address: hvk@sci.kun.nl

[1] M.M.J. Bischoff, T. Yamada, A.J. Quinn, R.G.P. van der Kraan, and H. van Kempen, Phys. Rev. Lett. **87**, 246102 (2001).
[2] A.R. Miedema, P.F. de Chatel, and F.R. de Boer, Physica B **100**, 1 (1980).
[3] J. Tersoff, Phys. Rev. Lett. **74**, 434 (1995).
[4] A. Davies, J.A. Stroscio, D.T. Pierce, J. Unguris, and R.J. Celotta, J. Magn. Magn. Mater. **165**, 82 (1997).
[5] E.L.D. Hebenstreit, W. Hebenstreit, M. Schmid, and P. Varga, Surf. Sci. **441**, 441 (1999).
[6] M. Schmid and P. Varga, in *The Chemical Physics of Solid Surfaces*, edited by D. P. Woodruff, Alloy Surfaces and Surface Alloys, Vol. 10 (Elsevier, Amsterdam, 2002).
[7] J.A. Stroscio, D.T. Pierce, A. Davies, R.J. Celotta, and M. Weinert, Phys. Rev. Lett. **75**, 2960 (1995).
[8] A. Biedermann, O. Genser, W. Hebenstreit, M. Schmid, J. Redinger, R. Podloucky, and P. Varga, Phys. Rev. Lett. **76**, 4179 (1996).
[9] T. Kawagoe, E. Tamura, Y. Suzuki, and K. Koike, Phys. Rev. B **65**, 024406 (2002).
[10] M.M.J. Bischoff, T. Yamada, A.J. Quinn, and H. van Kempen, Surf. Sci. **501**, 155 (2002).
[11] A. Davies, J.A. Stroscio, D.T. Pierce, and R.J. Celotta, Phys. Rev. Lett. **76**, 4175 (1996).
[12] P. Varga and M. Schmid, Appl. Surf. Sci. **141**, 287 (1998).
[13] J. Tersoff and D.R. Hamann, Phys. Rev. B **31**, 805 (1985).
[14] M.M.J. Bischoff, C. Konvicka, A.J. Quinn, M. Schmid, J. Redinger, R. Podloucky, P. Varga, and H. van Kempen, Phys. Rev. Lett. **86**, 2396 (2001).
[15] M. Pratzer, H.J. Elmers, M. Bode, O. Pietzsch, A. Kubetzka, and R. Wiesendanger, Phys. Rev. Lett. **87**, 127201 (2001).